Surface and interstitial Ti diffusion at the rutile TiO2(110) surface

Article

Accepted Version

Accepted version using RSC template- please check copyright etc.

Mulheran, P. A., Nolan, M., Browne, C. S., Basham, M., Sanville, E. and Bennett, R. A. ORCID: https://orcid.org/0000-0001-6266-3510 (2010) Surface and interstitial Ti diffusion at the rutile TiO2(110) surface. Physical Chemistry Chemical Physics, 12 (33). pp. 9763-9771. ISSN 1463-9076 doi: 10.1039/C002698K Available at https://centaur.reading.ac.uk/5776/

To link to this article DOI: http://dx.doi.org/10.1039/C002698K

Publisher: Royal Society of Chemistry

Surface and Interstitial Ti Diffusion at the Rutile TiO_2(110) Surface

P.A. Mulheran,*[a] M. Nolan*[b], C.S. Browne[c], M. Basham[d], E. Sanville[e] and R.A. Bennett[f]

Received (in XXX, XXX) Xth XXXXXXXXX 200X, Accepted Xth XXXXXXXXX 200X
First published on the web Xth XXXXXXXXX 200X
DOI: 10.1039/b000000x

Diffusion of Ti through the TiO_2 (110) rutile surface plays a key role in the growth and reactivity of TiO_2. To understand the fundamental aspects of this important process, we present an analysis of the diffusion of Ti adspecies at the stoichiometric TiO_2(110) surface using complementary computational methodologies of density functional theory corrected for on-site Coulomb interactions (DFT+U) and a charge equilibration (QEq) atomistic potential to identify minimum energy pathways. We find that diffusion of Ti from the surface to subsurface (and *vice versa*) follows an intersticialcy exchange mechanism, involving exchange of surface Ti with the 6-fold coordinated Ti below the bridging oxygen rows. Diffusion in the subsurface between layers also follows an interstitialcy mechanism. The diffusion of Ti is discussed in light of continued attempts to understand the re-oxidation of non-stoichiometric TiO_2(110) surfaces.

1. Introduction

Titanium dioxide is a technologically important material and has garnered considerable attention as a possible source of clean energy by photocatalytic water splitting, as a cleanup technology in waste streams and when combined with suitable supported metal catalysts as an environmental gas purifier. Titania also has applications in coatings and sensors[1]. Besides these applications, it is one of the most widely studied prototypical reducible metal oxides with the Ti having many stable oxidation states producing a complex structural phase diagram[2]. Stoichiometric TiO_2 has four polymorphs: rutile, anatase, brookite and cotunnite[3]. Nearly stoichiometric rutile shows two homologous series of planar bulk defects that self-assemble into crystallographic shear planes: Ti_nO_{2n-1} with ($4<n<10$) based on {121} directed planes; and ($16<n<\sim37$) based on {132}[4 - 6]. Stable reduced phases down to Ti_4O_7, a crystal structure with promising electrical characteristics[7], can also be formed. Ti_2O_3 is a corundum structured pure Ti^{3+} phase which also appears as a reduced surface phase on near stoichiometric rutile surfaces treated in vacuum[8]. The equilibrium phases make an interesting system in which to modify the electrical and structural characteristics of the oxide. The atomistic processes that allow the system to move, for example, from stoichiometric rutile to a self-assembled planar array of defects in the bulk upon reduction, are somewhat hidden from view. However, recent experimental work has highlighted some key constituents to the puzzle, notably by considering the reverse process, that is the re-oxidation of non-stoichiometric material[9 - 11].

The rutile (110) surface has been extensively investigated experimentally over a number of years by surface science techniques, and usually on electrically conducting bulk reduced crystals that have changed colour which indicates a non-stoichiometry. Early work on re-oxidation by Henderson suggested Ti interstitials were the key point defect in non-stoichiometric rutile[12]. Indeed Scanning Tunnelling Microscopy (STM) studies by Onishi and Iwasawa showed how these defects can move from bulk to surface to grow new surface phases, the so-called added row Ti_2O_3 reconstruction[8]. At elevated temperature, however, variable temperature STM revealed how the (110) surface of a reduced crystal re-grows new layers of TiO_2 (in contrast to Ti_2O_3) in a rather complex layer-by-layer fashion when exposed to oxygen[9, 10]. These studies show that the reduced crystal contains a solid solution of Ti interstitials that are mobile above ~473K and able to diffuse to the surface to react with the impinging oxygen (or other adsorbed species such as formate[13]). The relationship between the reduction and re-oxidation steps has been demonstrated by further experiments on the self-doping of titania crystals and ultra-thin films which show how deposited Ti adatoms can diffuse into the bulk as interstitials when annealed[14]. Ti interstitials and adatoms are therefore of paramount importance to the surface structures,[15] the surface chemistry[16] and the growth of titania, and it is desirable to have modelling schemes that can describe these species, their reactivity and their mobility[17]. Modelling schemes that accurately represent electronic and geometric structures are particularly challenging for non-stoichiometric materials with variable oxidation states.

The description of reduced rutile has been an active topic for many years, with much discussion as to whether the dominant species involved are Ti interstitials[15] or oxygen vacancies[18]. Both defects can produce the same signature in ultra violet photoemission spectroscopy and in density functional theory (DFT) simulations[19], i.e. reduced Ti^{3+} ions. However, this debate is not the reason we study Ti interstitials. Rather, given that these species are key to the growth of TiO_2 through their diffusion from bulk to the surface and reaction with oxygen, we are studying the diffusion of Ti interstitials as a first step to providing a deeper understanding of this process.

Reference 17 provides a thorough exploration of the diffusion of Ti and O ad-species on the rutile (110) surface using density functional theory (DFT) with the local density approximation (LDA). However, it is known that this approach will not describe well the localisation of d-electrons that are expected in reduced titania. Therefore we have undertaken a series of calculations using DFT+U to correct for on-site Coulomb interactions, providing a good comparator for the LDA results and allowing confrontation with experiment to assess the relative merits of the approaches. In particular, in recent work we have presented direct experimental valdiation of the DFT+U computational approach, applied in this paper. We studied self-doped titania films, characterising the electronic properties of surface adsorbed Ti[20]. We found that an approach such as DFT+U is indeed needed to interpret the experimental results and consistently describe the Ti^{3+} ions present in this system. The best agreement with the spectroscopy of the gap states induced by the adsorbed adatom is obtained with U=3eV. This result is consistent with the value of U assigned in calculations of oxygen vacancies in the (110) surface[21], which create a reduced surface Ti defect state in the band gap. These latter calculations share important similarities with B3LYP results[22] which also localise the Ti 3d states.

In this paper we employ experimentally benchmarked calculations of static structures[20] to consider the dynamical aspects of Ti adatom and interstitial mobility in the rutile (110) surface. We find key barriers and transition pathways in the surface and subsurface regions and explore their electronic structure. The results are contrasted with those of reference 17, and are found to be in much better agreement with experimental results. Furthermore, we believe the charge localisation we predict facilitates new physical insight into surface growth and reactivity.

In our work, the DFT+U methodology is used to investigate the stability and properties of the Ti interstitials, since it is known to provide a consistent description of reduced Ti[20,21]. To investigate the diffusion pathways between the various adatom and interstitial sites, of which there are many possibilities, we first employ atomistic calculations using the charge equilibration (QEq) methodology[17, 23-31]In order to provide a realistic set of minimum energy pathways (MEP) for full investigation with DFT+U, we consider the effectiveness of the QEq approach in describing the energy landscape of the defects, and find that some modification to the original model is required. The modification employed involves altering the degree of charge transfer between species in the model, in particular restricting the transfer to Ti species only. This change is grounded in our analysis of the DFT+U calculations, and is consistent with experimental observations. With the modified potential shown to describe interstitial Ti consistently, we then screen a number of diffusion pathways, and select the most energetically favourable for further quantification using constrained minimisation in DFT+U calculations. The QEq approach has the appealing quality of being able to describe defects such as Ti interstitials and their diffusion and is an appropriate method to use for modelling of the dynamics of Ti diffusion and reaction with oxygen to ultimately study the dynamics of TiO_2 growth.

The layout of the paper is as follows. In the following section, we describe the computational methodologies. In section 3 we present results, first for the structures and energies of the interstitials and adatoms using the DFT+U and atomistic QEq calculations, and describe the impact of our charge transfer modification on the latter. In Section 3.2 we present results for our Minimum Energy Pathways for diffusion in the selvedge. Discussions of our results, focussing on charge transfer during diffusion, follow in Section 4 along with conclusions for the implications of our results for experimental interpretation and future dynamical simulation of surface growth.

2. Methodology

2.1 DFT+U Calculations

All our first principles calculations are carried out in the framework of periodic plane wave density functional theory (DFT)[32]. In this approach, the valence electronic states are expanded in a basis of periodic plane waves, with an energy cut-off of 396 eV, while the core-valence interaction is treated using PAW potentials[33]. The PW91 exchange-correlation functional is used throughout. The surface is modelled as a finite thickness slab model with three-dimensional periodicity. Surface slabs along the z-direction (perpendicular to the surface) are separated using a vacuum thickness of ~10 ´. For the interstitial calculations, a single Ti is placed in two different sites in the first, second and third (bulk-like) subsurface O-Ti-O layers. Full relaxation is performed, except for the bottom O-Ti-O unit. We refer to our previous work for details of the Ti adatoms adsorbed at the rutile (110) surface[20].

The slab model is 6 O-Ti-O units deep with a (2×4) surface cell expansion, minimising periodic defect-defect interactions, and providing a concentration of adsorbed Ti atoms that matches the coverage used in self-doping experiments[20]. k-point sampling is at the Γ-point and the Methfessel-Paxton smearing scheme with a smearing parameter of 0.1 eV is used. As discussed in the introduction, an important aspect of these calculations concerns the theoretical description of the reduced Ti ions. Reduced Ti ions have partially occupied 3*d* shells, which can be difficult to describe with approximate DFT exchange-correlation functionals[21, 21, 34-37]. It has already been demonstrated that the DFT+U approach[38,39] can be successfully applied to study non-stiochiometric TiO_2[20,21, 34 - 37] and we continue to use DFT+U in this work. The formalism due to Dudarev *et al.*[39] as implemented in VASP is employed. The quantity (U – J) is used, where J is the exchange parameter. However, since the system is not magnetic, we set J to be zero, so that (U – J) ≡ U. From our previous work[20], U is set to 3 eV.

The charge density from the converged VASP calculations was partitioned to the ions using our own Bader analysis code[40], allowing comparisons to be made to the charge distributions predicted through the QEq approach described next.

2.2 QEq Calculations

The DFT+U methodology leads to stronger localisation of charges in non-stoichiometric or defective structures in comparison to standard DFT[20, 21]. This physical picture strengthens the possibility of using empirical potential schemes which employ charges fixed spatially to ion cores in the lattice and especially those models which have the flexibility to allow charges to move. One such leading scheme is the QEq methodology[23] which allows charge transfer between ions to minimise the electrostatic energy E_{es}, whilst including contributions from the charging energies for each ion which takes a parabolic form:

$$E_{es} = \sum_i (E_i^0 + \chi_i^0 q_i + J_i^0 q_i^2) + \sum_{ij} J_{ij} q_i q_j \quad (1)$$

Here χ_i^0 and J_i^0 are related to the ions' electronegativity and hardness. J_{ij} is the shielded Coulomb interaction between ions, the shielding being estimated by the overlap of s-type Slater orbitals. For any given ionic configuration, the charge q_i on the ions is adjusted to minimise eqn. (1) under the constraint of conserved total charge $\sum_i q_i = 0$, without moving the ionic positions. Once this equilibration has been achieved, the resultant forces on the ions can be used to move them as in usual minimisation or dynamics procedures[25]. The atomistic model for the material is completed by the addition of short-range potentials to represent the covalent bonding which is known to be significant for titania[1]. Hallil *et al* have developed a suitable model for titania, using a pair-functional form to describe Ti-O covalent bonds[28].

In our QEq calculations we use the same rutile surface slabs described above for the DFT+U calculations. The lattice parameters were fixed to bulk values, and the ion coordinates relaxed. For both DFT+U and the QEq calculations, results with larger cells, larger vacuum gaps, and with two adsorbed adatoms either side of the slab (for the Ti adatom calculations) produce essentially identical results; more details are in ref. 20. The geometry minimisations were performed using a conjugate gradient method and we use our own in-house code to perform all the QEq calculations.

Minimum Energy Pathways for the interstitial and adatom diffusion are created with the QEq atomistic potential using the nudged elastic band method[41]. Selected pathways are further investigated using constrained minimisation with DFT+U. Here the position of the migrating species is held fixed whilst the surrounding atoms are relaxed. This procedure is performed for each image along the pathway, thereby assessing the pathway's viability and obtaining another estimate of the activation energy.

3. Results

3.1 The structure and energy of interstitials in the (110) surface

In reference 20 we presented results for the Ti adatom at the rutile (110) surface. Two stable binding sites are possible, the more favourable of which positions the adatom between two bridging and one in-plane oxygen. Due to the symmetry, we referred to it as the *ih* site[20]. In this paper, we find it convenient to change our notation where this adsorption site will henceforth be labelled A; see Figure 1. An alternative stable adsorption site is possible where the adatom is positioned between 2 in- plane and one bridging oxygen, labelled site B in Figure 1 and throughout the paper (it was labelled *iv* in ref. 20).

Within our DFT+U methodology, we calculated that site A is 0.34eV lower in energy than site B, however, a barrier for diffusion between B to A is present since B is found to be stable upon relaxation.

An important aspect of the DFT+U approach is to relate the localisation of charge to the defect-induced gap state observed in experiment. A convenient representation is found by plotting the spin iso-surfaces for the four extra unpaired d-electrons present in the surface with adsorbed Ti. Following this scheme, we present in Figure 2 the spin iso-surfaces with interstitials in the first, second and third O-Ti-O layers beneath the (110) surface. These sites are all have the same symmetry as the adatom in site A. In Figure 1 these sites are indicated as Fi in the first layer, and as shown they tend to sit beneath in-plane oxygen in plan view rather than directly beneath the site A adatom. The adatoms in the corresponding site in layers 2 and 3 are referred to as Fii and Fiii in the following section. The spin density plots in figure 2 show reduced Ti ions present – in particular the interstitial Ti has a Ti^{3+} oxidation state and a small number of neighbouring Ti atoms are also reduced to Ti^{3+}. Note that the electrons introduced by Ti are predominantly localised. In previous work, using hybrid DFT[42], Finazzi *et al.* also showed the formation of localised Ti^{3+} ions when a Ti interstitial is present, giving good confidence in our use of DFT+U.

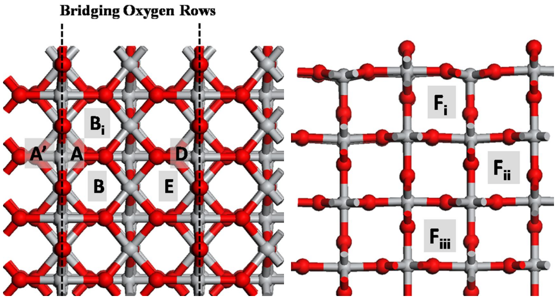

Fig.1 *Views of the (110) rutile surface indicating the adatom and interstitial sites used in this paper. Ti atoms are grey and O atoms are red. The Bridging oxygen rows are indicated with the dashed lines. Site A (and equivalents A' and D) is the adatom in its most favourable site, next to two bridging oxygen and one in-plane oxygen. Site B (and its equivalent E) is the adatom in its second favourable binding site next to one bridging and 2 in-plane oxygen. Site Fx is an interstitial site x O-Ti-O layers down with the same symmetry as site A; there is an alternative interstitial site Bx, with the same symmetry as site B.*

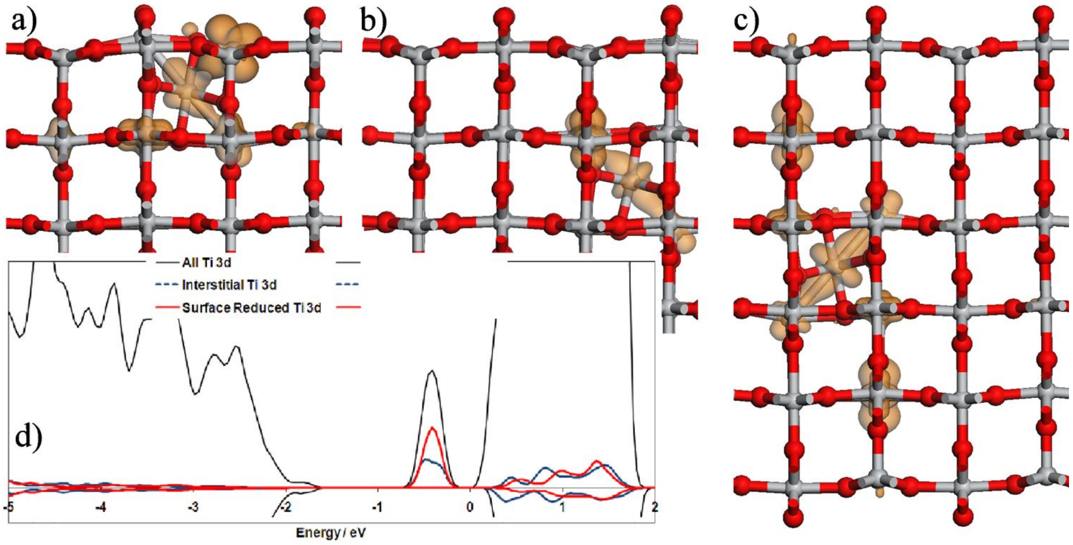

Fig2 *The spin density plots from the DFT+U interstitials (a) Fi, (b) Fii and (c) Fiii. Also shown in (d) is the projected electronic density of states, showing the Ti 3d derived gap state induced by the Fi interstitial*

Also shown in Figure 2 is the projected electron density of states for the Fi interstitial site. This shows the defect-induced gap state associated with Ti^{3+}, arising from the interstitial atoms and reduction of neighbouring lattice Ti. This contrasts to the split level found for the adatom in site A, where a Ti^{2+} signature is observed for the adatom, and a Ti^{3+} feature for an in-plane five-fold coordinated Ti^{3+}. In both cases, the remaining electron is spread across other lattice Ti. The corresponding results for the interstitial in the Bi site are not shown here but are broadly similar. They show surface 5-fold Ti reduced to 3+, the interstitial maintaining a 3+ oxidation state and the remaining charge spread over a small number of subsurface Ti.

We have also calculated the relaxed structure and energies of the interstitials using the QEq methodology[31]. In Figure 3 we show the relative energetics for the Ti adatom and interstitials from DFT+U and QEq calculations. With the energy of the A site adatom set to 0 eV for DFT+U and QEq, the figure shows the relative energetics of the B site adatom and the corresponding interstitial sites. Both DFT+U and QEq find the same stable sites, and furthermore the binding to the site A is the most favourable adatom site in both schemes, with an energy difference between A and B sites of 0.56eV in the QEq scheme respectively (*c.f* 0.34eV in DFT+U).

The difference in binding energy between the interstitial Fi and Bi sites (0.09eV and 0.07eV respectively) is much less marked than that between A and B in both the DFT+U and the QEq calculations, as might be anticipated since in bulk these sites would be identical by symmetry.

However, there is a marked difference between the energy of the adatom (A,B) and interstitial (Fi,Bi) sites calculated by DFT+U and the Hallil QEq model. The DFT+U calculation shows the interstitials are more energetically favourable than adatoms by 0.6eV and 0.8eV respectively for the A and B sites, whereas the QEq differences are very much larger at 2.5eV and 3.0eV. This is a significant difference in the energy landscapes of the models. Whilst our finding that Ti interstitials are more energetically favourable than adatoms agrees with experimental results for adatoms diffusing down into the bulk upon annealing[14], trapping them in the bulk by such a large amount as 2.5eV does not accord with the re-growth of reduced rutile at elevated temperature, even if oxygen ad-species promote the growth[9,10,15]. We conclude that the empirical QEq potential of Hallil *et al*[28] overestimates the adsorption energy of the interstitials with respect to the adatom energy.

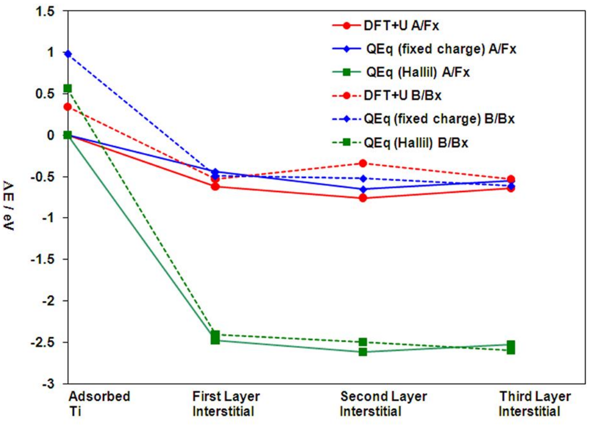

Fig.3 *Relative energies of different Ti sites from the DFT+U and QEq calculations. The energy of the Ti adatom in the A site is set to zero*

The reason for the discrepancy in the adatom-interstitial binding energy differences can be traced to the charge transfer occurring in the QEq potential at the (110) surface. In Figure 4 we show the QEq charges on the ions in the relaxed structures with the adatom in the surface A and B sites and the first layer insersitial Fi and Bi sites, as well as the labelling for Tables 1 and 2. In this figure, the radius of the ions reflects their excess charge (in e$^-$) over bulk values in order to provide a pictorial view of the charge distribution. For comparison, Bader analysis is used to partition the charge to the ions in the DFT+U results. The charges on the ions are given in Tables 1 and 2, and for clarity we also provide the pictorial view of the charge distributions for all calculations in the Supplementary Information.

Referring to Tables 1 and 2, it is clear that there is a qualitative difference between the behaviour of the Ti and the O atoms in the two approaches. In the case of the Ti, the QEq charges are broadly correlated with the Bader charges. In contrast, the distribution of charges on the O atoms do not correlate well between the calculations. In particular, the Bader analysis of the DFT+U reveals only small excess charges on the O atoms, within the limits of about +/- 0.1e^-, whereas the QEq model gives a much wider range of excess O charges in the range of about +/- 0.4e^-.

This charging of the oxygen nearest-neighbours by the Ti interstitial in the QEq model causes a favourable decrease in electrostatic energy with small penalties in self energy (see equation 1) and from the short range potential. These combine to lead to an elastic distortion in the surrounding lattice with ions moving closer together, screening the interstitials and significantly lowering the total energy. The response of the Ti adatom does not show such a strong effect since the adatom has fewer oxygen neighbours to charge.

The behaviour of the oxygen within the Hallil model suggests that the energetics of the QEq component underplay the costs of moving the charge both to and from the oxygen. To understand the consequences of this, we have repeated our calculations keeping the charge on all of the oxygens fixed to their bulk value of 1.26e^-, with only the Ti ions able to transfer charge between themselves using the original charging self-energies[28]. We show in Figure 3 how the energy landscape of the defects, measured relative to the energy of the adatom in site A in each model, is now in much better agreement with the DFT+U results.

Table 1 The excess charge dQ, measured in units of e^-, over bulk values for the ions labelled in Figs. 4a and 4b using the Hallil QEq potential, DFT+U and fixed O- charge QEq.

A adatom	Hallil QEq	DFT+U	Fixed O QEq
T1	*0.775*	*0.585*	*0.825*
T2	*0.215*	*0.074*	*0.348*
T3	*0.010*	*-0.007*	*-0.056*
O1	*0.370*	*0.127*	0.0
O2	*0.047*	*0.000*	0.0
B adatom	**Hallil QEq**	**DFT+U**	**Fixed O QEq**
T1	*0.812*	*0.990*	*0.825*
T2	*0.109*	*0.399*	*0.130*
T3	*0.273*	*0.006*	*0.420*
O1	*0.343*	*0.139*	0.0
O2	*0.011*	*0.016*	0.0
O3	*-0.355*	*-0.073*	0.0

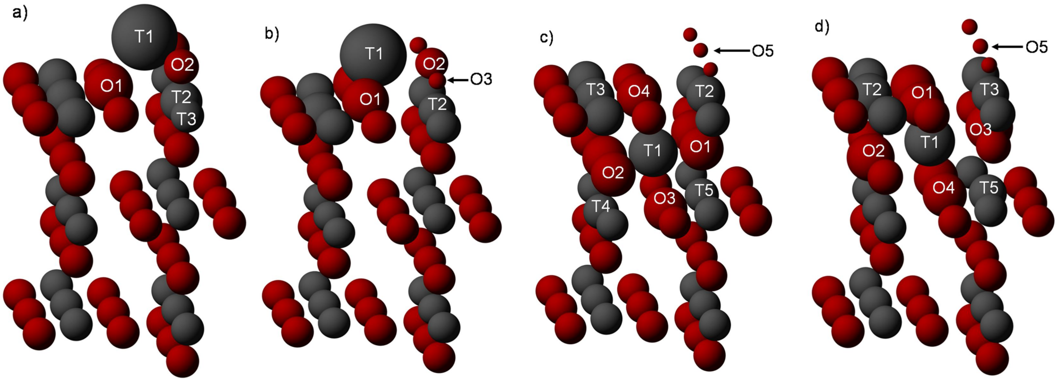

Fig. 4 *(a) Hallil model QEq results for the A adatom site; (b) Hallil model QEq results for the B site;(c) Hallil model QEq results for the Fi site and (d) Hallil model QEq results for the Bi site. The oxygen are red and the titanium dark grey. The size of the ions in all images represent how much excess charge dQ (e^-) is associated with the ion in comparison to its bulk charge (specifically radius scales as 1+1.3dQ.). The values of dQ for the labelled ions are given in Tables 1 and 2. Only a section of the full cell used in the calculations is show for clarity, with the upper surface being the free one with the exposed bridging oxygen.*

In support of the physical basis of this modification to the QEq model, experimental data for the core-level shifts in x-ray photoelectron spectroscopy of stoichiometric $TiO_2(110)$, Ti adatom doped $TiO_2(110)$, and added row Ti_2O_3 reconstructed $TiO_2(110)$ are presented in the Supporting Information. All cases show very similar O1s lineshapes with no spectral features attributable to large variances in oxygen charge state. This confirms that the charge transfer to and from the oxygen atoms of the $TiO_2(110)$ surface upon Ti adsorption predicted by our calculations should be minimal.

3.2 Minimum Energy Pathways for Ti interstitial Diffusion

Detailed results for NEB calculations of Ti diffusion with the QEq potentials have previously been presented in reference 31, to which we refer for further details. A summary of the activation energies of feasible diffusion pathways is given in Table 3, obtained with the modified (fixed oxygen charge) QEq model. From these, we select the most favourable pathways for further investigation with DFT+U.

The first pathway we consider for the diffusion between adatom and first layer interstitial is A-Fi via exchange with a

6-fold coordinated lattice Ti underneath the bridging oxygen row. In Figure 5 we show the energies of the images along the relaxed NEB pathway, using the starting site A adatom QEq energy as a convenient zero of energy. For alternate images along the path, we apply the constrained minimisation in DFT+U and plot the relaxed energies of the images alongside the original QEq values, using the DFT+U energy of site A as a convenient zero of energy. This procedure allows a direct comparison of a Minimum Energy Pathway in both models. It is apparent that the activation energy for the pathway is similar in both models (0.97eV for the QEq versus 0.83eV in DFT+U). Furthermore, the shape of the pathway energy plots is similar, indicating the QEq saddle point is geometrically similar to the DFT+U one. For convenience, we also show in Figure 5 the DFT+U geometry at some key points on the path and will return to this point in a later section.

Table 2 The excess charge dQ, measured in units of e^-, over bulk values for ions labelled in Figs. 4c and 4d due to interstitial insertion.

Fi interstitial	Hallil QEq model	DFT+U	Fixed oxygen-charge QEq
T1	*0.417*	*0.178*	*0.767*
T2	*0.166*	*0.072*	*0.025*
T3	*0.191*	*0.331*	*0.336*
T4	*0.091*	*0.047*	*0.286*
T5	*0.050*	*0.034*	*0.178*
O1	*0.288*	*0.065*	*0.0*
O2	*0.309*	*0.097*	*0.0*
O3	*0.279*	*0.087*	*0.0*
O4	*0.311*	*0.132*	*0.0*
O5	*-0.415*	*-0.091*	*0.0*
Bi interstitial			
T1	*0.409*	*0.216*	*0.748*
T2	*0.269*	*0.445*	*0.438*
T3	*0.104*	*0.032*	*-0.032*
T4	*0.032*	*0.014*	*0.189*
T5	*0.118*	*0.224*	*0.296*
O1	*0.284*	*0.105*	*0.0*
O2	*0.348*	*0.082*	*0.0*
O3	*0.337*	*0.079*	*0.0*
O4	*0.259*	*0.103*	*0.0*
O5	*-0.409*	*-0.080*	*0.0*

Table 3 *Energy barriers (eV) for the forward and backward moves found using the NEB method using the fixed oxygen-charge variant of the QEq model; the figures in brackets are for the DFT+U estimates (see text).*

	Forward	Backward
A-Fi (exchange)	*0.97 (0.83)*	*1.41 (1.40)*
A-Fi (direct)	*2.20 (----)*	*2.64 (----)*
B-Bi (exchange)	*0.47 (0.66)*	*1.94 (1.55)*
B-Bi (direct)	*0.96 (----)*	*2.43 (----)*
Bi-Bii (exchange)	*1.31 (1.00)*	*1.35 (0.60)*
Bi-Bii (direct)	*2.02 (----)*	*2.06 (----)*
Fi-Fii (exchange)	*1.31 (0.76)*	*1.53 (0.84)*
A-B	*1.12 (0.83)*	*0.14 (0.52)*
A-D	*3.49 (----)*	*3.49 (----)*
B-E	*1.83 (----)*	*1.83 (----)*
Bi-Fi	*0.81 (0.72)*	*0.77 (0.63)*

Table 3 shows that an alternative low-energy pathway exists for adatoms to diffuse to interstitial sites, that of B-Bi via exchange with an in-plane 5-fold coordinated Ti in the surface trench. In Figure 6 we again compare the MEP found using the NEB method and the modified QEq with that obtained using constrained minimisation in DFT+U along the same pathway, using the starting site B energies in each model as convenient zeros of energy. Again we note the similarity in the shapes of the energy plots along this pathway, lending confidence that the empirical potential provides a pathway that is also feasible in the DFT+U methodology. The activation energy is lower in the QEq scheme at 0.47eV compared to 0.66eV for DFT+U. However, the energy landscape shows that the relative energy of site B over site A is higher in the modified QEq (0.98eV) than in the DFT+U (0.31eV). This high energy starting point has the effect of distorting the pathway, lowering the activation energy and moving the saddle point towards the interstitial site Bi.

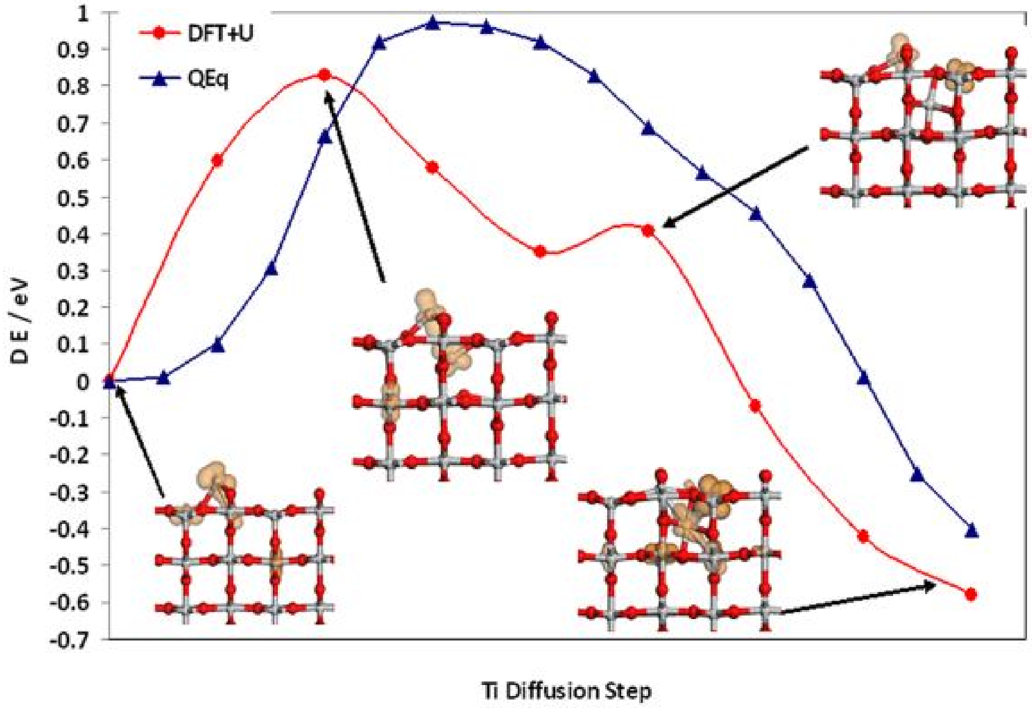

Fig. 5 *Minimum Energy Pathways for A-Fi via 6-fold exchange. The structure indicated at selected steps along the MEP includes the DFT+U spin density to show how the charge localisation changes during the migration process.*

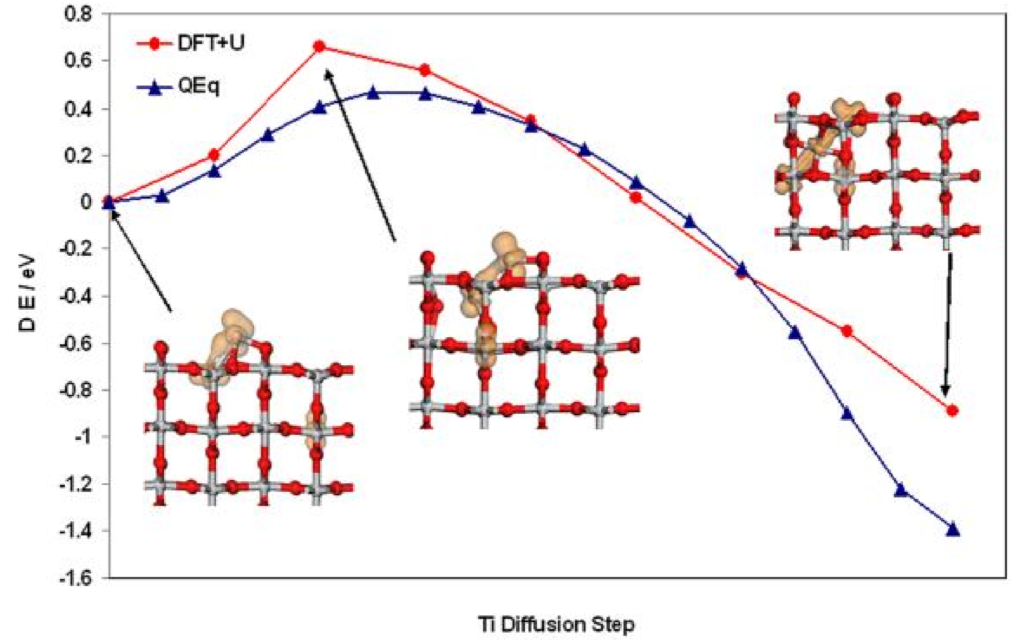

5 **Fig. 6** *Minimum Energy Pathways for B-Bi via 5-fold exchange. The structure indicated at selected steps along the MEP includes the DFT+U spin density to show how the charge localisation changes during the migration process*

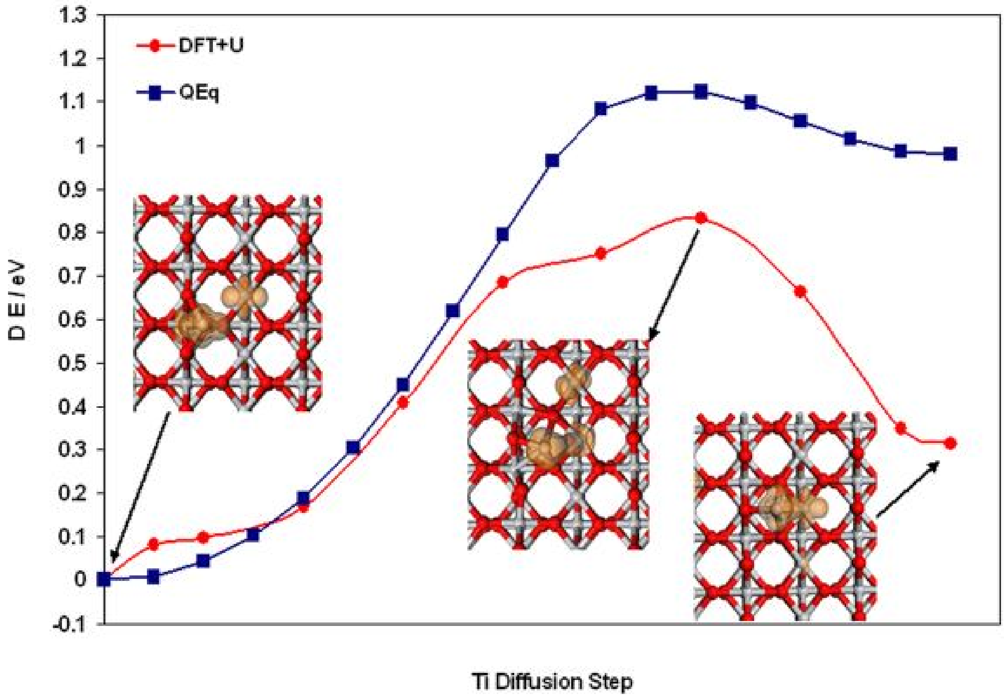

Fig. 7 *Intra-layer Minimum Energy Pathways from the surface A to surface B site. The structure indicated at selected steps along the MEP includes the DFT+U spin density to show how the charge localisation changes during the migration process*

While diffusion from a surface B site has a lower activation barrier than from the A site, we need to follow migration of the Ti adatom from the surface A site to the surface B site. To this end, Figure 7, shows the MEP for an adatom diffusing between sites A and B, which has a barrier of 1.12 eV (QEq)/ 0.83 eV (DFT+U). This emphasises the point that site B has a rather high energy in the modified QEq model, compared to the DFT+U calculations (see above) and the computed energy barriers also indicate that diffusion from the A to the B site will not be a frequent event. Of particular interest is whether this distorts the activation energy of the adatom to interstitial diffusion. In the modified QEq, the composite pathway A-B-Bi is dominated by the first step with the activation energy 1.12eV, a little higher than the activation energy of 0.97eV for the aforementioned A-Fi interstitial move. In the DFT+U model, the composite pathway again is dominated by the A-B activation energy 0.83eV, which is the same activation energy as for the A-Fi interstitial move. Therefore it seems both pathways are competitive in our calculations, although the A-B-Bi pathway has two steps, whereas the A-Fi pathway has a single step. The preference appears to be for the A-Fi pathway, although A-B-Bi would be possible on experimental timescales at the relevant growth temperature >400K[9,10].

To complete our analysis of the interstitial diffusion at the surface, we also study the MEP in the models with subsurface diffusion (data not shown). The intra-layer Bi-Fi move in the first subsurface layer corresponds to the B-A adatom move at the surface. Again the trends in the curves are satisfactorily correlated, showing an almost symmetric shape, with an activation energy of 0.72 eV from DFT+U, lower than in the surface A-B move. Table 3 shows a summary of the MEP's including diffusion pathways between subsurface layers. The interstitial move Bi-Bii via exchange with a lattice Ti is found to be favoured over the direct move. The DFT+U activation energy for this diffusion is 1.00 eV, comparing with 1.31 eV for the modified QEq. The Fi-Fii exchange diffusion pathway has a barrier of 0.76eV in DFT+U in good agreement with the value used in ref. 15. The pathways for out diffusion of interstitials torwards the surface from bulk are also given in the backwards pathway column of Table 3.

4. Discussion and Conclusions

The results in this paper present a thorough picture of the interaction of Ti atoms with the rutile (110) surface and provide useful insights into the near surface diffusion of interstitial Ti. The Ti adatom is most stable in the surface A site. Although interstitial sites are determined to be more stable, there is a barrier for diffusion from the surface to the interstitial sites (and *vice versa*). The most favourable pathway is the surface A site to interstitial Fi site (and *vice versa)*. In this pathway, the Ti adatom moves towards a 6-fold coordinated lattice Ti site, which in a concerted motion, moves to the interstitial site. For this pathway, figure 5 shows the structures of some intermediate steps, clearly showing the concerted motion of both the adatom and the lattice Ti.

In the inserts of figure 5 we show the computed spin density for critical steps. In the A site, the Ti adatom is in the +2 oxidation state, a surface 5-fold coordinated Ti atom is in the +3 oxidation state and the remaining electron of the four introduced by neutral Ti, is spread over a small number of Ti atoms. In the interstitial Fi, site, the interstitial Ti and surrounding reduced Ti atoms have a +3 oxidation state. At the highest point on the MEP, we see that the originally 6-fold coordinated Ti atom has moved towards the interstitial site and has picked up some charge so that the original adatom now has a +3 oxidation state as does a subsurface Ti atom (the previously reduced 5-fold surface Ti atom is now a Ti^{4+} ion). A second, local, maxima in the MEP arises when the adatom and two surface 5-fold coordinated Ti atoms have a +3 oxidation state and the interstitial is a Ti^{4+} ion. By the final stages, one of the surface Ti^{3+} ions is oxidised to Ti^{4+} and the interstitial Ti is now a Ti^{3+} ion and the system relaxes to a lower energy configuration.

Thus, the Ti diffusion pathway shows a number of changes of Ti oxidation states for the diffusing atoms and for neighbouring Ti atoms. Our results show that the barrier in the MEP arises at the point at which two (large) Ti^{3+} ions are rather close to each other, which is an energetically unfavourable situation. Once past this step on the MEP, the reduced Ti atoms are no longer so close to each other and migration of Ti proceeds. It is interesting to note that the interstitals donate charge to the 5 fold Ti in the surface and that these electrons will be available to adsorbates to aid dissociative adsorption[13]. For the re-oxidation of the surface by O_2 one may expect these sites to be especially reactive and lead to the creation of O adatom adsorption close to the Ti interstitials. These may then facilitate the out-diffusion of Ti interstitials through the exchange pathways identified here modified by the more stable transition and final states.

For the Ti diffusion pathways in figures 6, 7, we also show the structure and spin densities at important points along the MEP. In all these migration pathways, we observe that the maximum in the barrier is obtained when reduced Ti species come closest to each other along the migration pathway.

We can compare the diffusion barriers we find with DFT+U to those found using bare DFT (LDA) in reference 17. In that work, the barrier for the A-Fi interstitialcy move is 1.60eV (compared to 0.83eV here) and for the B-Bi interstitialcy move it is 1.76eV (c.f. 0.66eV). The contrast for the reverse moves, i.e. the out-diffusion of interstitials to the surface, is even more marked, since the interstitials are highly favoured energetically over adatoms in LDA by 1.91eV (c.f. 0.53eV here). These contrasts appear to be due to the role electron localisation plays in stabilising the structures and diffusion pathways, and as stated above, the correct description of this will be important to the understanding of surface dissociative adsorption.There is no doubt that experiments support the lower diffusion barriers found in the DFT+U calculations here. Indeed, some of these diffusion pathways have been (indirectly) measured. In particular a barrier of 0.44 ± 0.06 eV was found for the in-diffusion of submonolayer of Ti deposited on near stoichiometric $TiO_2(110)$[11]. This measurement follows Ti^{3+} core-level shifted features in photoemission spectroscopy and is thus sensitive to diffusion through several monolayers (the escape depth of photoemitted electrons) but is in reasonable agreement with the lower energy pathways described here. The bulk diffusion has been previously calculated to follow an intersticialcy mechanism with a barrier of 0.225 eV (significantly lower than the barrier of 0.37 eV along the c-axis)[43].

A comparison of results for the DFT+U and QEq descriptions of adsorbed Ti and Ti interstitials shows that the modified QEq potential gives results that are in reasonable agreement with the DFT+U results. The relative stabilities of the various adatom and interstitial sites are in good agreement, as are the charge distributions, as evidenced by plotting the Bader charges for the Ti adatom and interstitial sites. We aim to use the QEq model for studying the interaction of Ti with oxygen and the growth of TiO_2 layers, full simulation of which is presently beyond the reach of first principles simulations. The comparison of Ti migration pathways from DFT+U and QEq shows that the potential provides a very good description of Ti migration and will be suitable for dynamic simulation of surface growth processes, in particular where substoichiometric Ti is present. In addition, the QEq potential can also be used for screening of potential structure and diffusion pathways for full simulation of selected structures with first principles approaches.

Acknowledgements

PAM, CSB and MB acknowledge support from EPSRC grants EP/C524349 and GR/T18738 and the University of Reading UK. MN acknowledges support from Science Foundation Ireland, “EMOIN” grant number SFI 09/SIRG/I1620 and computing resources provided by the SFI and Higher Education Authority Funded Irish Centre for High End Computing.

Notes and references

[a] *Department of Chemical and Process Engineering, University of Strathclyde, 75 Montrose Street, Glasgow G1 1XJ, UK*
Fax: +44 (0)141 548 2539; Tel: +44 (0)141 548 2385; E-mail: paul.mulheran@strath.ac.uk
[b] *Tyndall National Institute, University College Cork, Lee Maltings, Cork, Ireland*
Fax: +353-21-4270271; Tel: +353-21-490-4063; E-mail: michael.nolan@tyndall.ie
[c] *Department of Physics, University of Reading, Whiteknights, Reading, RG6 6AF, UK.*
[d] *Diamond Light Source Ltd, Diamond House, Harwell Science and Innovation Campus, Didcot OX11 0DE, UK*
[e] *Department of Mathematical Sciences, Loughborough University, Loughborough LE11 3TU, UK*
[f] *School of Chemistry, University of Reading, Whiteknights, Reading RG6 6AD, UK. Fax: +44 (0)1189750203; Tel: +44 (0)1183788559; E-mail: r.a.bennett@reading.ac.uk*

References

1. U. Diebold, Surf. Sci. Rep. 2003, 48, 53
2. G.V. Samsonov, The Oxide Handbook, IFI/Plenum Press, New York 1982.
3. L.S. Dubrovinsky, N.A. Dubrovinskaia, V. Swamy, J.Muscat, N.M. Harrison, R. Ahuja, B. Holm, B. Johansson, Nature 2001, 410, 653.
4. R.A. Bennett, S. Poulston, P. Stone and M. Bowker, Phys. Rev. B 1999, 59 10341.
5. G.S. Rohrer, V.E. Henrich and D.A. Bonnell, Science 1990, 250, 1239.

6. G.S. Rohrer, V.E. Henrich and D.A. Bonnell, Surf. Sci. 1992, 278,146.
7. M. Marezio, A. Gauzzi, F. Licci and E. Gilioli, Physica C 2000, 338, 1.
8. H. Onishi and Y. Iwasawa, Phys. Rev. Lett. 1996, 76, 791.
9. P. Stone, R. A. Bennett, and M. Bowker, New Journal of Physics 1999, 1, 8.
10. R. D. Smith, R. A. Bennett, and M. Bowker, Phys. Rev. B 2001, 66, 035409.
11. M. Bowker and R. A. Bennett, J. Phys.: Condens. Matter 2009, 21, 474224; J. Phys.: Condens. Matter 2010, 22, 059801.
12. M.A. Henderson, Surf. Sci. 1999, 419, 174.
13. R.A. Bennett, P. Stone and M. Bowker, Faraday. Discuss. 1999, 114, 348.
14. N. D. McCavish and R. A. Bennett, Topics in Catalysis 2005, 36, 11.
15. S. Wendt P. T. Sprunger, E. Lira, G. K. H. Madsen, Z. Li, J. Ø. Hansen, J. Matthiesen, A. Blekinge-Rasmussen, E. Lægsgaard, B. Hammer, and F. Besenbacher, Science 2008, 320, 1755.
16. R.A. Bennett, P. Stone and M. Bowker, Faraday Discuss. 1999, 114, 267.
17. E. J. Sanville, L. J. Vernon, S. D. Kenny, R. Smith, Y. Moghaddam, C. Browne and P. Mulheran, Phys. Rev. B 2009, 80, 235308.
18. C. M. Yim, C. L. Pang and G. Thornton, Phys. Rev. Lett. 104, 036806, 2010
19. Di Valentin et al. J. Phys. Chem. C 113, 20543, 2009
20. M. Nolan, S.D. Elliott, J.S. Mulley, R.A. Bennett, M. Basham and P.A. Mulheran, Phys. Rev. B 2008, 77, 235424.
21. B. J. Morgan and G. W. Watson, Surf. Sci. 2007, 601, 5034.
22. C. Di Valentin, G. Pacchioni, and A. Selloni, Phys. Rev. Lett. 2006, 97, 16680.
23. A. K. Rappe and W. A. Goddard, J. Phys. Chem 1991, 95, 3358.
24. X. W. Zhou, H. N. G. Wadley, J.-S. Filhol, and M. N. Neurock, Phys. Rev. B 2004, 69, 035402.
25. V. Swamy and J. D. Gale, Phys. Rev. B 2000, 62, 5406.
26. V. Swamy, J. Muscat, J. D. Gale, and N. M. Harrison, Surf. Sci. 2002, 504, 115.
27. B. S. Thomas, N. A. Marks, and B. D. Begg, Phys. Rev. B 2004, 69, 144122.
28. A. Hallil, R. Tétot, F. Berthier, I. Braems and J. Creuze, Phys. Rev. B 2006, 73, 165406.
29. B. S. Thomas and N. A. Marks, Phys. Rev. B 2007, 76, 167401
30. A. Hallil, R. Tétot, F. Berthier, I. Braems and J. Creuze, Phys. Rev. B 2007, 76, 167402.
31. P.A. Mulheran, C.S. Browne and Y. Moghaddam, Mol. Sim., 2009, 35, 532
32. G. Kresse and J. Hafner, Phys. Rev. B, 1994, 49, 14251; G Kresse and J. Furthmüller, Comp. Mat. Sci. 1996, 6, 15
33. P. E. Blöchl, Phys. Rev. B 1994, 50, 17953; D. Joubert and G. Kresse, Phys. Rev. B 1999, 59, 1758.
34. Y. F. Zhang, W. Lin, Y. Li, K. N. Ding, and J. Q. Li, J. Phys. Chem. B, 2005, 109, 19270.
35. A. I. Poteryaev, A. I. Lichtenstein, and G. Kotliar, G. Phys. Rev. Lett., 2004, 93, 086401.
36. R. Pentcheva, and W. E. Pickett, Phys. Rev. B, 2006, 74, 035112.
37. D. D. Cuong, B. Lee K. M. Choi H. S. Ahn, S. Han, and J. Lee, Phys. Rev. Lett., 2007, 98, 115503.
38. V. I. Anisimov, J. Zaanen, and O. K. Andersen, Phys. Rev B, 1991, 44, 943.
39. S. L. Dudarev, G. A. Botton, S. Y. Savrasov, C. J. Humphreys, and A. P. Sutton, Phys. Rev. B, 1998, 57, 1505.
40. E. Sanville, S. D. Kenny, R. Smith, and G. Henkelman, J. Comp. Chem. 2007, 28, 899.
41. G. Henkelman and H. Johnsson, J. Chem. Phys. 113:9978 (2000)
42. E. Finazzi, C. Di Valentin and G. Pacchioni,J. Phys. Chem. C 113, 3382, 2009
43. H. Iddir, S. Öğüt,P. Zapol and N.D.. Browning, Phys. Rev. B, 2007, 75, 073203